Complex anomalous Hall effect of CoGd alloy near the magnetization compensation temperature

Ting Fu,[1] Shuangfeng Li,[1] Xiaoyu Feng,[1] Yongwei Cui,[1] Jiguang Yao,[1] Bo Wang,[1] Jiangwei Cao,[1] Zhong Shi,[2] Desheng Xue,[1] and Xiaolong Fan[1,*]

[1]*Key Laboratory for Magnetism and Magnetic Materials of the Ministry of Education, Lanzhou University, Lanzhou 730000, People's Republic of China*

[2]*Shanghai Key Laboratory of Special Artificial Microstructure and School of Physics Science and Engineering, Tongji University, Shanghai 200092, People's Republic of China*

(Received 30 November 2020; accepted 3 February 2021; published 26 February 2021)

In this article, the temperature-dependent complex Hall effect near the magnetization compensation temperature of CoGd alloy films is systematically studied. We find anomalies of Hall loops with characteristics similar to the topological Hall effect (THE), which is usually considered to indicate the occurrence of topological spin texture. However, the THE is ruled out by detailed magnetic and transport measurements on CoGd alloy films with different composition ratios. After considering the influence of the spin-flop effect and the inhomogeneity of the components naturally formed in the ferrimagnetic CoGd alloy, we constructed a phenomenological model that can explain the complex Hall effect near the magnetization compensation point without relying on the THE. The main result is helpful for explaining the microscopic magnetic properties and transport properties of rare-earth transition metal ferrimagnetic alloys near the compensation point.

DOI: 10.1103/PhysRevB.103.064432

I. INTRODUCTION

In rare-earth (RE) transition-metal (TM) ferrimagnetic alloys $TM_{100-X}RE_X$, the atomic magnetic moments of TM and RE exhibit antiferromagnetic exchange coupling. The magnitude of the net magnetization M (angular momentum J) can be adjusted over a wide range by varying the temperature and component ratio, and this parameter can reach zero at the compensation temperature T_M (T_A) or compensation concentration X_M (X_A) [1–15]. Because the magnetic properties of ferrimagnets are similar to those of antiferromagnets, but their magnetic states can easily be detected at the magnetization compensation point [14], TM-RE alloys show excellent application value in recent studies. For instance, the spin-orbit torque (SOT) effective field and the efficiency of magnetization switching driven by SOT are maximized at T_M and X_M [3,5–8,11–13], which makes these materials good candidates for SOT applications. In addition, the speed of current-induced domain-wall movement and that of the SOT driving its magnetization switching can break the theoretical limit of traditional ferromagnets and reach a large value at T_A or X_A [9,10,15], which improves the energy efficiency and operating speed of the system and promotes the realization of ultrafast and energy-saving spintronic devices.

In addition, the topological Hall effect (THE), the fingerprint of topological spin texture, was found near T_M in TM-RE alloys [9,16,17], which drew more attention to TM-RE alloy films. The THE means that the Hall resistivity has an extra term because of the appearance of topological spin texture, which can be indicated by an extra hump in the Hall curve [18,19]. The THE has been widely observed in magnetic perovskites [20], Heusler alloys [21], and multilayer structures with strong interface Dzyaloshinskii–Moriya interactions (DMIs) [22,23]. Nevertheless, for TM-RE alloys, the extra hump only appears near T_M and at specific concentrations, according to previous reports [17], and there is a lack of corresponding characterization such as spin-resolved scanning tunneling microscopy, neutron scattering in momentum space, Lorentz electron microscopy techniques in real space [24], or any direct proof. Therefore, the origin of the extra hump is still ambiguous. In addition, the inhomogeneous components due to the oxidation of RE [25,26], the reversed polarity of the anomalous Hall effect (AHE) loop [6,7] and the reduced spin-flop field around T_M [27] all also contribute to complex behaviors in the Hall curve.

To clarify the origin of the complex Hall curve around T_M, we systematically studied the change in the Hall loop with respect to temperature in CoGd alloys with different component ratios. Then, we found aberrant humps that appeared in all of our samples around T_M. However, precise magnetic transport measurements eliminated the contribution of the THE. Based on the models proposed by Kan *et al.* for $SrRuO_3$ [28], we established an extended model to qualitatively explain the emergence of aberrant humps after considering the inhomogeneity of the sample components.

II. SAMPLE FABRICATION AND MEASUREMENT

In our experiment, we deposited stacks of $Ta(1nm)/Co_{100-X}Gd_X(20nm)/Pt(5nm)$ by dc magnetron sputtering on Si/SiO_2 substrates, where X is the percentage of Gd atoms in the CoGd alloy. The Ta (1 nm) in the lower layer and Pt (5 nm) in the upper layer formed buffer and protective

*fanxiaolong@lzu.edu.cn

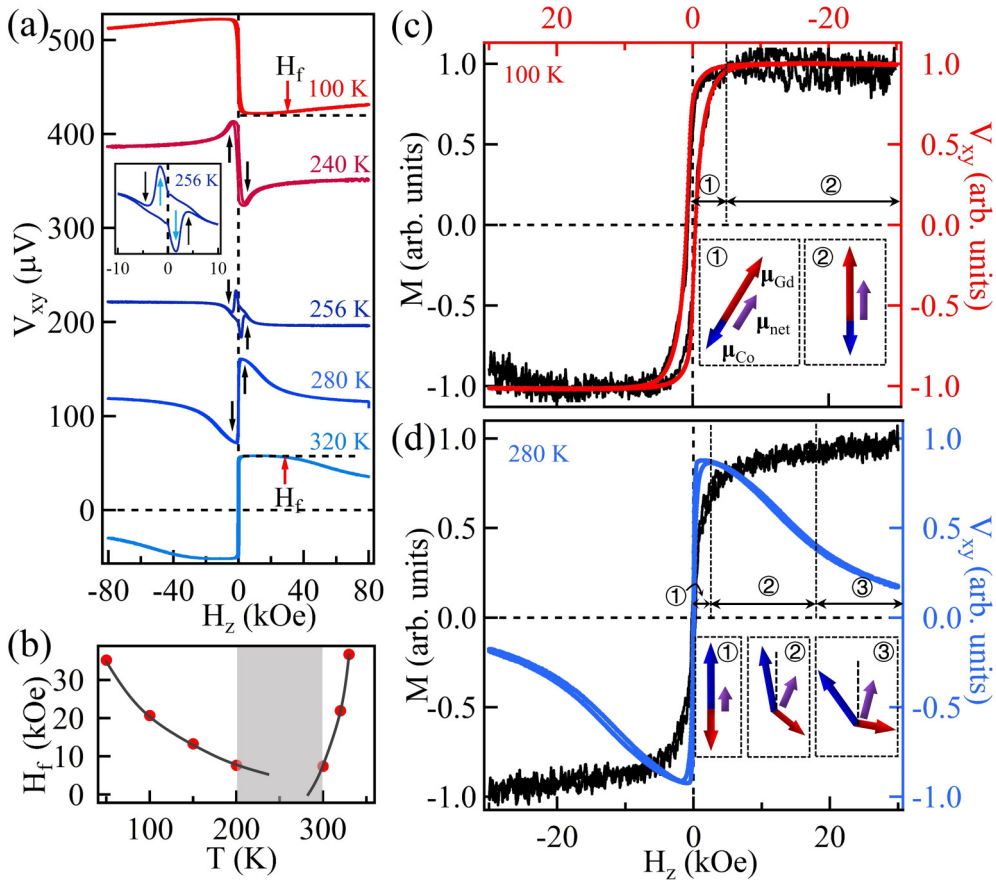

FIG. 1. (a) The Hall loops of $Co_{79.7}Gd_{20.3}$ at different temperatures, which are shifted longitudinally for convenience. The positions of the spin-flop field H_f are indicated by the red arrows. The abnormal humps indicated by the black arrows are observed at 240, 256, and 280 K, and we call them the type-I humps. The inset shows a locally enlarged loop at 256 K, where the humps marked by the blue arrows are defined as the type-II hump. (b) Temperature-dependent H_f for $Co_{79.7}Gd_{20.3}$. The black line is a guide for the eye, and the type-I hump appears in the temperature range marked by the gray shaded area. The cross-reference of *M-H* loop and the Hall loop for $Co_{79.7}Gd_{20.3}$ at (c) 100 K and (d) 280 K. The loop at 100 K is reversed for comparison. The magnetic moment states within the corresponding magnetic field range are shown in dashed boxes, where the red, blue, and purple arrows represent $\boldsymbol{\mu}_{Gd}$, $\boldsymbol{\mu}_{Co}$, and $\boldsymbol{\mu}_{net}$, respectively.

layers, which reduced the influence of substrate roughness on the film and prevented the film from being oxidized. The base pressure of the main chamber was better than 2×10^{-7} Torr, and the Ar pressure was maintained at 5×10^{-3} Torr during sputtering. The CoGd layer was deposited by cosputtering, the sputtering power density of the Gd sources was fixed, and the concentration ratio of Gd atoms to Co atoms was adjusted by changing the power density of the Co sources. The component ratio of the samples was characterized by a plasma emission spectrometer. The testing platform based on VersaLab was used to measure the hysteresis loop. The Hall loops were measured using a self-built transport testing system with a Cryogenic-J4440 cryofree vector magnet.

III. MEASUREMENT OF HALL LOOP IN A LARGE MAGNETIC FIELD

Temperature-dependent Hall loop measurements were performed in the range of 50 to 380 K, and the maximum applied magnetic field was 80 kOe. Figure 1(a) shows the results of $Co_{79.7}Gd_{20.3}$. The polarity of the Hall loop reverses between 240 and 280 K, indicating that the net magnetic moment $\boldsymbol{\mu}_{net}$ changes from the phase dominated by the atomic magnetic moment of Gd, $\boldsymbol{\mu}_{Gd}$ (240 K), to that dominated by Co, $\boldsymbol{\mu}_{Co}$ (280 K), and T_M is within this range [6,7]. The reverse of the Hall loop exhibits a gradational transition, where an aberrant Hall signal can be observed. Taking the curve at 280 K as an example, aberrant humps are indicated by the black arrow in the figure. The Hall voltage V_{xy} is approximately zero under zero field, rapidly increases and reaches its maximum value under a small field, and then decreases with increasing external magnetic field. At 240 K, the curve shows similar features but with the opposite polarity. Note that the aberrant humps in the Hall loop are similar to the THE caused by the noncoplanar spin texture in antiferromagnetic and ferrimagnetic insulators, which was studied by Cheng, Shao, *et al.* [29–32]. Moreover, a similar hump can be observed in $Co_{80.7}Gd_{19.3}$ and $Co_{79.1}Gd_{20.9}$, as shown in the Supplemental Material S1 [33]. We think that the type of hump observed in our experiments is not caused by topological spin texture, since the polarity of the humps reverses with that of the AHE loop from the Gd-dominated phase (240 K) to the Co-dominated phase (280 K). The polarity of the hump caused by the THE is only determined by the topological charge of net magnetic moment in

the topological spin texture [34], which should not be reversed with temperature.

It is known that a ferrimagnet undergoes a spin-flop transition if the magnetic field reaches the critical value H_f, where $\boldsymbol{\mu}_{Co}$ and $\boldsymbol{\mu}_{Gd}$ change from collinear to noncollinear [27]. When the magnetic anisotropy is weak, the spin-flop field $H_f \approx n_{RT}|M_T - M_R|$, where n_{RT} is the intersublattice exchange field parameter and M_T (M_R) is the magnetization of the TM (RE) sublattice [35]. As shown in Fig. 1(a), H_f can be clearly observed in the curves of 100 and 320 K, as indicated by red arrows. We summarize the temperature-dependent H_f in Fig. 1(b), which suggests that the values of H_f approach zero in the vicinity of T_M. Since the hump only appears around T_M, we believe that the hump is just a consequence of the spin-flop when H_f approaches a zero field.

To prove this conjecture, we compare the out-of-plane hysteresis loop (M-H) with the Hall loop for $Co_{79.7}Gd_{20.3}$. Since the M-H loop depends on the out-of-plane component of $\boldsymbol{\mu}_{net}$ and the Hall loop only depends on that of $\boldsymbol{\mu}_{Co}$, the divergence in between indicates spin-flop (or noncollinearity between Gd and Co). As shown in Fig. 1(c), the magnetization M and Hall voltage V_{xy} show the same variation tendencies as H_z at 100 K, which is far from T_M, suggesting that $\boldsymbol{\mu}_{Co}$, $\boldsymbol{\mu}_{Gd}$, and $\boldsymbol{\mu}_{net}$ are collinear. At 280 K, near T_M, the Hall loop becomes completely different from the $M - H_z$ loop. The magnetization increases monotonically with increasing H_z, but V_{xy} increases and then decreases with H_z, which indicates that spin-flop occurs with a very small applied magnetic field. The insets in Figs. 1(c) and 1(d) show schematic diagrams of magnetic moment states with different magnetic fields, where the red, blue, and purple arrows represent $\boldsymbol{\mu}_{Gd}$, $\boldsymbol{\mu}_{Co}$, and $\boldsymbol{\mu}_{net}$, respectively. According to the above analysis, this hump is caused by the noncollinear $\boldsymbol{\mu}_{Gd}$ and $\boldsymbol{\mu}_{Co}$ due to the appearance of spin-flop under a very small magnetic field. The data for $Co_{79.1}Gd_{20.9}$ are shown in the Supplemental Material S2 [33] and support the same conclusion.

IV. MEASUREMENT OF HALL LOOP IN SMALL MAGNETIC FIELD

Another kind of aberrant hump can be observed on the Hall loop at 256 K, as shown in the locally enlarged inset of Fig. 1(a). The fundamental difference of this type of hump is the hysteretic dependence. Then, we define the aberrant hump discussed earlier as the type-I hump and the hump here as the type-II hump. To obtain more detailed features, we measure the Hall loops with a smaller temperature interval close to T_M, and the results of $Co_{79.7}Gd_{20.3}$ and $Co_{80.7}Gd_{19.3}$ are shown in Figs. 2(a) and 2(b), respectively. Taking the data of 254 K in Fig. 2(a) as an example, a maximum occurs when H_z decreases from a positive field to −2.6 kOe and a minimum appears when H_z increases from negative field to 2.6 kOe. The shape of the overall Hall loop shows inverse symmetry with respect to H_z. In Fig. 2(b), the Hall loop of $Co_{80.7}Gd_{19.3}$ in the range of 202 to 208 K shows similar characteristics, but the polarity of the humps is opposite. Note that the tilt background of the loop is caused by spin-flop rather than the ordinary Hall effect, which is absent for the loops far from T_M, such as the curves of 50 and 350 K.

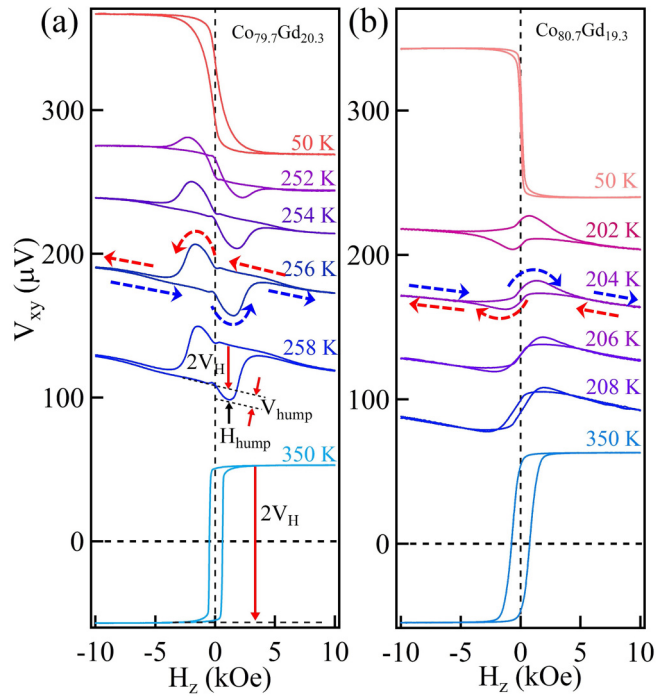

FIG. 2. The Hall loops of (a) $Co_{79.7}Gd_{20.3}$ and (b) $Co_{80.7}Gd_{19.3}$ at different temperatures, which are shifted longitudinally for convenience. The red and blue dotted lines with arrows represent the direction of the magnetic field scan. The definitions of V_H, V_{hump}, H_{hump}, and H_C are indicated.

The main features of the type-II hump observed here are quite similar to that of the THE caused by the topological spin texture reported for MnGe, FeGe, and MnSi with an asymmetric crystal structure [36–38], Heusler alloys [21,39,40], $SrIrO_3/SrRuO_3$ thin films [41], CoTb alloys [17], etc. If we arbitrarily declare that the type-II hump results from the THE, then the DMI in $Co_{80.7}Gd_{19.3}$/Pt and $Co_{79.7}Gd_{20.3}$/Pt would be opposite. According to previous reports, the adjacent heavy-metal layer with strong spin-orbit coupling [29,30,32,34] and the transverse gradient of the component distribution [26] introduce DMI and stabilize the topological spin texture in ferrimagnetic films. However, it is hard to explain why a 1% increase in Gd concentration results in opposite DMI in the two samples.

To analyze the cause of the type-II hump, we summarize their main characteristics. We define H_{hump} as the field at which the hump is positioned in the positive field and V_{hump} as the amplitude of the humps, as indicated in Fig. 2(a). For $Co_{79.7}Gd_{20.3}$ ($Co_{80.7}Gd_{19.3}$), the hump only appears within the temperature range of 248–266 K (190–210 K). In this range, H_{hump} decreases (increases) with increasing temperature, and the value of V_{hump} is negative (positive) and shows a minimum (maximum) at approximately 254 K (203 K), as shown in Figs. 3(a)–3(d). In addition, the values of the anomalous Hall voltage V_H are plotted in Figs. 3(c) and 3(d) for comparison. Note that we define V_H as $[V(+0) - V(-0)]/2$ around T_M rather than the saturated Hall voltage in the positive field because of the occurrence of spin-flop. We find that, for all the samples, the maximum amplitude of V_{hump} always appears

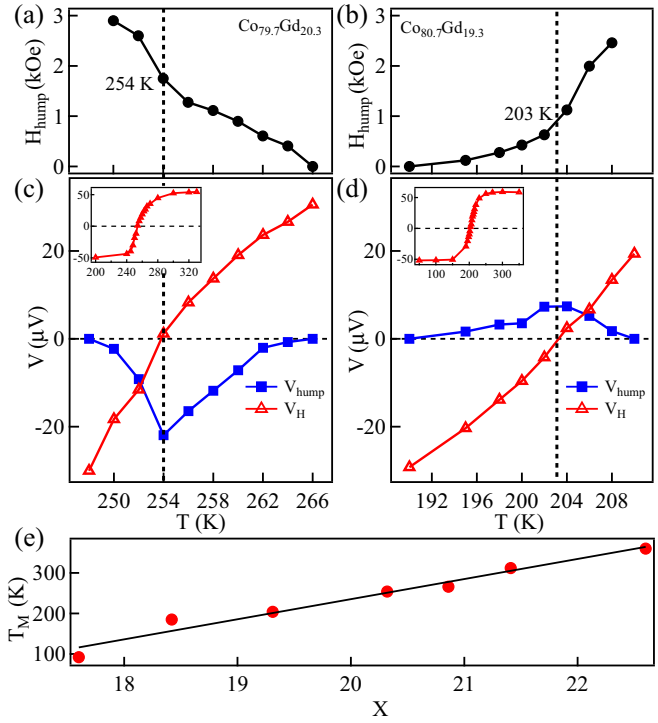

FIG. 3. Temperature-dependent H_{hump} of (a) $Co_{79.7}Gd_{20.3}$ and (b) $Co_{80.7}Gd_{19.3}$. Temperature-dependent V_{hump} and V_{H} of (c) $Co_{79.7}Gd_{20.3}$ and (d) $Co_{80.7}Gd_{19.3}$. The insets show V_{H} versus temperature within larger temperature range. (e) The dependence of magnetization compensation temperature T_{M} on Gd atom concentration X. The black line is a linear fit of the data.

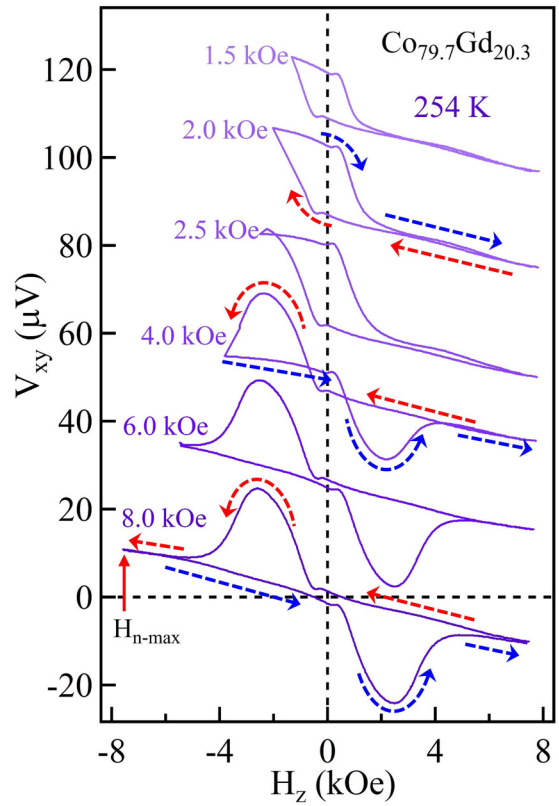

FIG. 4. The minor loops of $Co_{79.7}Gd_{20.3}$ at 254 K. The maximum positive magnetic field is fixed at 8.0 kOe and the maximum negative magnetic field $H_{\text{n}-\text{max}}$ changes from 1.5 to 8.0 kOe.

at the temperature at which V_{H} is zero. In other words, if we still declare that the type-II hump results from the THE, the number of skyrmions only shows a maximum at T_{M} values of the films with different compositions. However, the appearance of skyrmions is a complex accordance between the energy of anisotropy, DMI, exchange, and the Zeeman effect. Therefore, it is unlikely that these two phenomena ($V_{\text{H}} = 0$ and the appearance of skyrmions) occur at the same time, considering that there is a 270 K difference in T_{M} when X changes from 17.3 to 22.6, as shown in Fig. 3(e).

In addition, we measure the minor Hall loop of $Co_{79.7}Gd_{20.3}$ at 254 K to study the hysteresis characteristics of the hump, as shown in Fig. 4. When the minor loop is measured, the magnetic field starts with an 8 kOe decrease to $H_{n-\text{max}}$ and then returns to 8 kOe. The humps are essentially hysteretic, and their emergence in the positive field seems to depend on whether $H_{n-\text{max}}$ surpasses the magnetic field -2.6 kOe, at which the other hump exhibits a maximum. However, this hysteresis dependency cannot be the same as the concept of the skyrmion formation leading to the THE [28]. As a result of the many doubts raised above, we believe that the formation of the type-II hump is not caused by the existence of the topological spin texture in the CoGd thin film.

V. A MODEL BASED ON INHOMOGENEOUS COMPOSITION

In the following, we explain the above experimental results based on a simple model inspired by the model proposed by Kan *et al.* for $SrRuO_3$ [28], in which we only introduce an inhomogeneous composition in the CoGd films and do not consider the topological spin textures. Considering the temperature-dependent coercivity determined from the experiment, all the characteristics of the humps can be clearly understood.

First, assuming that a CoGd alloy has an average Gd atom concentration X_{S} and average magnetization compensation temperature $T_{\text{M}-\text{S}}$, the concentration distribution of Gd follows a Gaussian function. When $T \ll T_{\text{M}-\text{S}}$ ($T \gg T_{\text{M}-\text{S}}$), the magnetization is dominated by Gd (Co), which is indicated by the red (blue) regions in Figs. 5(a) and 5(e), and the corresponding Hall loop has negative (positive) polarity. Around $T_{\text{M}-\text{S}}$, the Gd- and Co-dominant phases coexist due to the concentration distribution, and the proportion of the Gd- (Co-) dominant phase gradually decreases (increases) with increasing temperature due to increasing X_{M}, as shown in Figs. 5(a)–5(e). For each phase, the magnitude of the AHE resistivity basically does not change with temperature [6,7,42], and the AHE voltage in the Gd-dominant phase V_{H}^{Gd} and that in the Co-dominant phase V_{H}^{Co} only depend on their proportions. Therefore, the temperature-dependent AHE voltage for each phase can be qualitatively depicted, as in Figs. 5(f) and 5(i).

Another important parameter in our model is the coercivity of each phase. Based on the experimental data shown in Fig. 6 and previous reports [2,7,11,43–48], the coercivity of the Gd- (Co-) dominant phase H_{c}^{Gd} (H_{c}^{Co}) increases (decreases) with temperature, and its gradient changes with

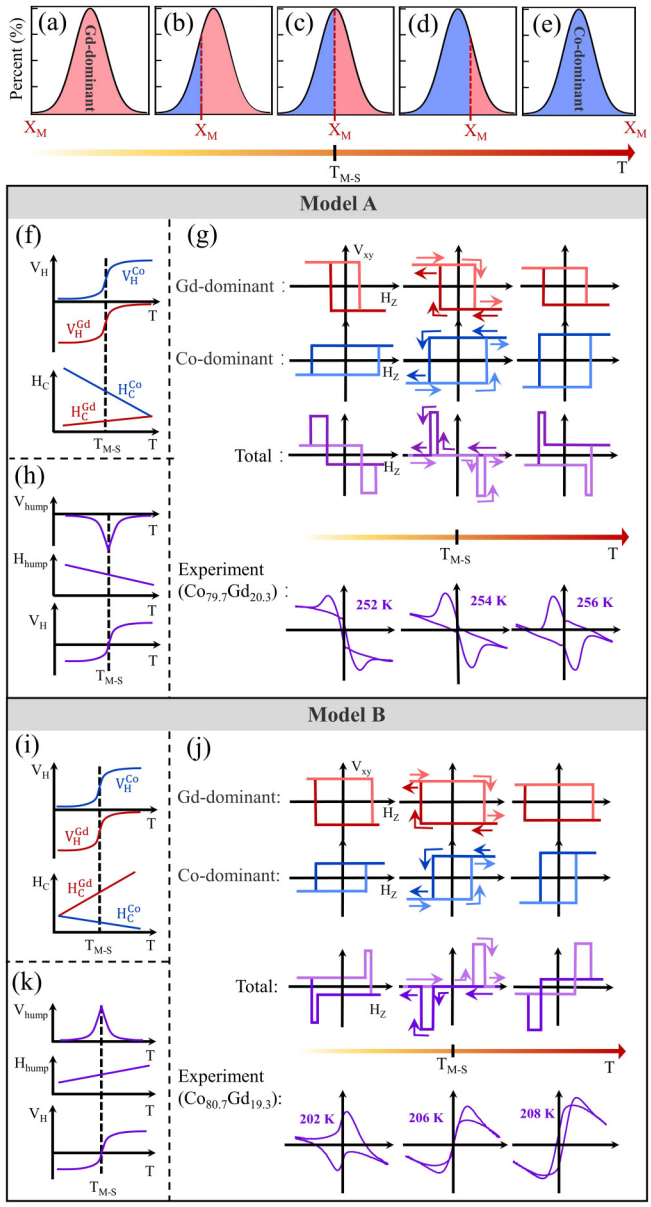

FIG. 5. Schematic diagram of a model based on inhomogeneous composition. (a)–(e) The relative variation in the proportions of the two phases with increasing temperature for a sample with average concentration X_S. Model A and Model B correspond to the cases of $Co_{79.1}Gd_{20.9}$ and $Co_{80.7}Gd_{19.3}$, respectively.

temperature differ for samples with different proportions of components. Note that the relative values and gradient changes with temperature of H_c^{Gd} and H_c^{Co} are critical for determining the characteristics of the type-II humps. From Fig. 6, we obtain that $H_c^{Gd} < H_c^{Co}$ ($H_c^{Gd} > H_c^{Co}$) and that H_c^{Gd} (H_c^{Co}) has smaller gradient changes with temperature for $Co_{79.1}Gd_{20.9}$ ($Co_{80.7}Gd_{19.3}$) around T_{M-S}. We simplify these relationships to be linear, as shown in the bottom panels of Figs. 5(f) and 5(i).

Based on the above considerations, we believe that the total AHE loop exhibited by the sample with a concentration distribution is a linear superposition of the contributions of two individual phases. We draw out the rectangular AHE

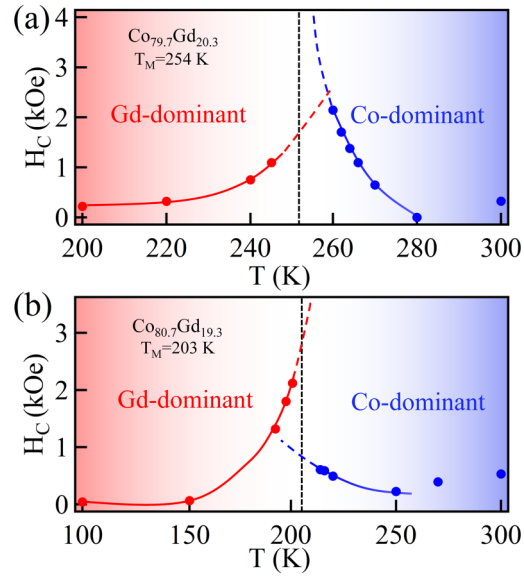

FIG. 6. Temperature-dependent H_C of (a) $Co_{79.7}Gd_{20.3}$ and (b) $Co_{80.7}Gd_{19.3}$. The red and blue lines are to guide the eyes.

loops of the two phases and their linear superpositions, as shown in Figs. 5(g) and 5(j). Clearly, the type-II hump appears only in the magnetic-field range between two individual switches of each phase. The calculated curves are highly consistent with our experiments, except for the influence of spin-flop, which results in a tilt background. Moreover, the characteristics of the humps can be clearly understood with the model as follows:

(1) The hump appears only near T_{M-S} for the sample, and its polarity depends on the relative values of the coercivity of the two phases. When $H_c^{Gd} < H_c^{Co}$ ($H_c^{Gd} > H_c^{Co}$), the polarity of the hump is negative (positive), independent of the polarity of the total AHE in the sample. The amplitude of the hump is $|V_{hump}| = |V_H^{Co} - V_H^{Gd} - |V_H^{Co} + V_H^{Gd}||$. The temperature-dependent V_{hump} is predicted, as shown in Figs. 5(h) and 5(k), which always show extreme values at T_M.

(2) The field position of the hump, $H_{hump} = (H_c^{Gd} + H_c^{Co})/2$, and the trend of H_{hump} with temperature are determined by the rate of the temperature-dependent $H_c^{Gd} + H_c^{Co}$, as shown in Figs. 5(h) and 5(k).

(3) The rectangular loop between two humps is the total AHE voltage, whose value $V_H = V_H^{Co} + V_H^{Gd}$ changes from negative to positive with increasing temperature, and $V_H = 0$ at T_{M-S}, as shown in Figs. 5(h) and 5(k).

In conclusion, the schematic loops in Figs. 5(g) and 5(j) are consistent with the presented experimental data of $Co_{79.7}Gd_{20.3}$ and $Co_{80.7}Gd_{19.3}$. For $Co_{82.4}Gd_{17.6}$ and $Co_{81.6}Gd_{18.4}$, the case is the same; see the Supplemental Material S3 [33] for details. Note that the rectangular AHE loops used in Figs. 5(g) and 5(j) are not necessary for the appearance of the hump in our model. For $Co_{78.6}Gd_{21.4}$ and $Co_{77.4}Gd_{22.6}$, with weak perpendicular magnetic anisotropy and in-plane anisotropy, respectively, similar humps have been observed, which are caused by the difference in saturation magnetization (equivalent demagnetization) of two phases [4,7,11,45,48], see Supplemental Material S4 [33] for details. The appear-

ance of the hump in films without PMA is further support for our exclusion of the THE since PMA is crucial for the formation of skyrmions [9,22,34]. Finally, we demonstrate that the type-II hump mainly comes from the inhomogeneity of the composition of our samples, and its emergence does not definitely indicate the formation of topological spin texture. We notice that the similar anomalies of AHE caused by inhomogeneity have been recently reported not only in $SrRuO_3$ [28,49–52], but also in Co/Pd multilayers [53,54].

Moreover, the inhomogeneity of the Gd composition can be evaluated by our model. As shown in Fig. 3(e), T_M changes by approximately 50 K when the concentration of Gd changes by one percent. On the other hand, the type-II hump appears in the temperature range of 20 K for $Co_{79.7}Gd_{20.3}$ and $Co_{80.7}Gd_{19.3}$, so we can roughly estimate that the inhomogeneity of Gd is approximately 0.4 percentage points.

VI. CONCLUSIONS

In the study of the temperature-dependent Hall loop of CoGd alloys with different component ratios, two types of aberrant humps were observed near the magnetization-compensation temperature. The type-I hump occurs under a large magnetic field and is caused by decreasing spin-flop field near the compensation point. The type-II hump appears in a small magnetic field with hysteresis features and exhibits characteristics similar to the THE introduced by topological spin texture. We exclude the THE through detailed experimental analysis and then construct a model based on the fact that composition inhomogeneity occurs in CoGd alloy films. This model can qualitatively explain all the characteristics of the type-II hump, at least for the samples with T_M in the range of 90 to 360 K in our experiment. Therefore, in TM-RE ferrimagnetic alloys, the additional hump in the Hall loop must be carefully considered, and one should avoid excessive attribution to the THE. The main result is helpful for extending our knowledge of the micromagnetism and complex transport properties of TM-RE ferromagnetic alloy films near the magnetization compensation point. Moreover, since inhomogeneity is inevitable in the fabrication of multielement materials, more attention should be paid to abnormal surprises at the critical points, especially in thin films.

ACKNOWLEGDMENTS

This project was supported by National Natural Science Foundation of China (Grants No 91963201, No. 11674142, No. 11774259, and No. 12074285), the Program for Changjiang Scholars and Innovative Research Team in University (Grant No. IRT-16R35), and the 111 Project under Grant No. B20063. We would like to thank AJE (www.aje.com) for English language editing.

[1] I. A. Campbell, J. Phys. F. **2**, L47 (1972).
[2] C. D. Stanciu, A. Tsukamoto, A. V. Kimel, F. Hansteen, A. Kirilyuk, A. Itoh, and T. Rasing, Phys. Rev. Lett. **99**, 217204 (2007).
[3] J. Finley and L. Liu, Phys. Rev. Appl. **6**, 054001 (2016).
[4] X. Jiao, Z. Zhang, and Y. Liu, Spin. **06**, 1650003 (2016).
[5] R. Mishra, J. Yu, X. Qiu, M. Motapothula, T. Venkatesan, and H. Yang, Phys. Rev. Lett. **118**, 167201 (2017).
[6] W. Seung Ham, S. Kim, D.-H. Kim, K.-J. Kim, T. Okuno, H. Yoshikawa, A. Tsukamoto, T. Moriyama, and T. Ono, Appl. Phys. Lett. **110**, 242405 (2017).
[7] K. Ueda, M. Mann, P. W. P. de Brouwer, D. Bono, and G. S. D. Beach, Phys. Rev. B **96**, 064410 (2017).
[8] S.-G. Je, J.-C. Rojas-Sánchez, T. H. Pham, P. Vallobra, G. Malinowski, D. Lacour, T. Fache, M.-C. Cyrille, D.-Y. Kim, S.-B. Choe, M. Belmeguenai, M. Hehn, S. Mangin, G. Gaudin, and O. Boulle, Appl. Phys. Lett. **112**, 062401 (2018).
[9] M. Mann, L. Caretta, F. Büttner, K. Ueda, B. Pfau, C. M. Günther, P. Hessing, A. Churikova, C. Klose, M. Schneider, D. Engel, C. Marcus, D. Bono, K. Bagschik, S. Eisebitt, and G. S. D. Beach, Nat. Nano. **13**, 1154 (2018).
[10] S. A. Siddiqui, J. Han, J. T. Finley, C. A. Ross, and L. Liu, Phys. Rev. Lett. **121**, 057701 (2018).
[11] R. C. Bhatt, L.-X. Ye, Y.-C. Luo, and T.-h. Wu, J. Appl. Phys. **125**, 113902 (2019).
[12] Y. Xu, H. Wu, P. Deng, Q. Pan, S. A. Razavi, K. Wong, L. Huang, B. Dai, Q. Shao, G. Yu, X. Han, J. C. Rojas-Sanchez, S. Mangin, and K. L. Wang, Adv. Mater. **31**, 1901681 (2019).
[13] Z. Zheng, Y. Zhang, X. Feng, K. Zhang, J. Nan, Z. Zhang, G. Wang, J. Wang, N. Lei, D. Liu, Y. Zhang and W. Zhao, Phys. Rev. Appl. **12**, 044032 (2019).
[14] J. Finley and L. Liu, Appl. Phys. Lett. **116**, 110501 (2020).
[15] Z. Zhu, K. Cai, J. M. Lee, R. Mishra, L. Ren, S. D. Pollard, P. He, G. Liang, K. L. Teo, and H. Yang, Nat. Electron. **3**, 37 (2020).
[16] K. M. Song, S. Woo, X. Zhang, Y. Zhou, M. Ezawa, X. Liu, S. Finizio, J. Raabe, N. J. Lee, S. I. Kim, S. Y. Park, Y. Kim, J. Y. Kim, D. Lee, O. Lee, J. W. Choi, B. C. Min, H. C. Koo, and J. Chang, Nat. Commun. **9**, 959 (2018).
[17] L. Liu, J. Yu, J. Deng, C. Zhou, H. Liu, F. Poh, and J. Chen, J. Magn. Magn. Mater. **487**, 165316 (2019).
[18] P. Bruno, V. K. Dugaev, and M. Taillefumier, Phys. Rev. Lett. **93**, 096806 (2004).
[19] H. Yoshizawa, Y. O. Y. Taguchi, N. Nagaosa, and Y. Tokura, Science. **291**2573 (2001).
[20] L. Vistoli, W. Wang, A. Sander, Q. Zhu, B. Casals, R. Cichelero, A. Barthélémy, S. Fusil, G. Herranz, S. Valencia, R. Abrudan, E. Weschke, K. Nakazawa, H. Kohno, J. Santamaria, W. Wu, V. Garcia, and M. Bibes, Nat. Phys. **15**, 104 (2019).
[21] P. Swekis, A. Markou, D. Kriegner, J. Gayles, R. Schlitz, W. Schnelle, S. T. B. Goennenwein, and C. Felser, Phys. Rev. Mater. **3**, 013001(R) (2019).
[22] M. Raju, A. Soumyanarayanan, A. L. Gonzalez Oyarce, A. K. C. Tan, M. Y. Im, A. P. Petrovic, P. Ho, K. H. Khoo, M. Tran, C. K. Gan, F. Ernult, and C. Panagopoulos, Nat. Mater. **16**, 898 (2017).
[23] A. Yagil, M. Raju, A. Soumyanarayanan, A. K. C. Tan, A. Almoalem, F. Ma, O. M. Auslaender, and C. Panagopoulos, Nat. Commun. **10**, 696 (2019).
[24] L. Wu and J. Y. Zhang, arXiv:1812.09847v6.

[25] D. Lee, J. Kim, K. J. Lee, B. K. Ju, H. C. Koo, B. C. Min, and O. Lee, Sci. Rep. **8**, 6017 (2018).
[26] M. Haruta, D. H. Kim, H. W. Ko, G. Go, H. J. Park, T. Nishimura, D. Y. Kim, T. Okuno, Y. Hirata, Y. Futakawa, H. Yoshikawa, W. Ham, S. Kim, H. Kurata, A. Tsukamoto, Y. Shiota, T. Moriyama, S. B. Choe, K. J. Lee, and T. Ono, Nat. Mater. **18**, 685 (2019).
[27] J. Becker, A. Tsukamoto, A. Kirilyuk, J. C. Maan, T. Rasing, P. C. M. Christianen, and A. V. Kimel, Phys. Rev. Lett. **118**, 117203 (2017).
[28] D. Kan, T. Moriyama, K. Kobayashi, and Y. Shimakawa, Phys. Rev. B. **98**, 180408(R) (2018).
[29] A. J. Lee, A. S. Ahmed, N. Bagués, B. A. McCullian, A. M. A. Thabt, A. Perrine, P.-K. Wu, J. R. Rowland, M. Randeria, P. C. Hammel, D. W. McComb, and F. Yang, Nano Lett. **19**, 5683 (2019).
[30] Q. Shao, Y. Liu, G. Yu, S. K. Kim, X. Che, C. Tang, Q. L. He, Y. Tserkovnyak, J. Shi, and K. L. Wang, Nat. Electron **2**, 182 (2019).
[31] M. W. Daniels, W. Wang, Z. Liao, Y. Zhao, J. Wang, G. Koster, G. Rijnders, C. Z. Chang, D. Xiao, and W. Wu, Nat. Mater. **18**, 1054 (2019).
[32] A. J. Lee, A. S. Ahmed, J. Flores, S. Guo, B. Wang, N. Bagués, D. W. McComb, and F. Yang, Phys. Rev. Lett. **124**, 107201 (2020).
[33] See Supplemental Material S1, S2, and S3 at http://link.aps.org/supplemental/10.1103/PhysRevB.103.064432 for additional details and characterization of other samples, and S4 for the data and model for the samples without perpendicular magnetic anisotropy.
[34] G. Chen, W. Jiang, K. Liu, J. Zang, S. G. E. te Velthuis, and A. Hoffmann, Phys. Rep. **704**, 1 (2017).
[35] R. J. Radwański, Physica. **142**, 57 (1986).
[36] A. Neubauer, C. Pfleiderer, B. Binz, A. Rosch, R. Ritz, P. G. Niklowitz, and P. Boni, Phys. Rev. Lett. **102**, 186602 (2009).
[37] N. Kanazawa, Y. Onose, T. Arima, D. Okuyama, K. Ohoyama, S. Wakimoto, K. Kakurai, S. Ishiwata, and Y. Tokura, Phys. Rev. Lett. **106**, 156603 (2011).
[38] S. X. Huang and C. L. Chien, Phys. Rev. Lett. **108**, 267201 (2012).
[39] G. Dubuis, B. M. Ludbrook, A. H. Puichaud, B. J. Ruck, and S. Granville, Sci. Rep. **7**, 13620 (2017).
[40] V. Kumar, N. Kumar, M. Reehuis, J. Gayles, A. S. Sukhanov, A. Hoser, F. Damay, C. Shekhar, P. Adler, and C. Felser, Phys. Rev. B **101**, 014424 (2020).
[41] Q. Qin, L. Liu, W. Lin, X. Shu, Q. Xie, Z. Lim, C. Li, S. He, G. M. Chow, and J. Chen, Adv. Mater. **31**, 1807008 (2019).
[42] K.-J. Kim, T. Okuno, T. Tono, S. Kim, T. Moriyama, H. Yoshikawa, A. Tsukamoto, and T. Ono, Appl. Phys. Exp. **9**, 073001 (2016).
[43] D. J. Webb, A. F. Marshall, Z. Sun, T. H. Geballe, and R. M. White, IEEE Trans. Magn. **24**, 588 (1988).
[44] S. Demirtas, R. E. Camley, and A. R. Koymen, Appl. Phys. Lett. **87**, 202111 (2005).
[45] M. Binder, A. Weber, O. Mosendz, G. Woltersdorf, M. Izquierdo, I. Neudecker, J. R. Dahn, T. D. Hatchard, J. U. Thiele, C. H. Back, and M. R. Scheinfein, Phys. Rev. B **74**, 134404 (2006).
[46] N. Bergeard, A. Mougin, M. Izquierdo, E. Fonda, and F. Sirotti, Phys. Rev. B **96**, 064418 (2017).
[47] T. H. Pham, S. G. Je, P. Vallobra, T. Fache, D. Lacour, G. Malinowski, M. C. Cyrille, G. Gaudin, O. Boulle, M. Hehn, J. C. Rojas-Sánchez, and S. Mangin, Phys. Rev. Appl. **9**, 064032 (2018).
[48] J.-J. Wang, W. Tang, H.-P. Xie, K. Wang, and G.-H. Guo, Acta Phys. Pol. A. **137**, 368 (2020).
[49] D. Kan, K. Kobayashi, and Y. Shimakawa, Phys. Rev. B **101**, 144405 (2020).
[50] D. Kan, T. Moriyama, and Y. Shimakawa, Phys. Rev. B **101**, 014448 (2020).
[51] G. Kimbell, P. M. Sass, B. Woltje, E. K. Ko, T. W. Noh, W. Wu, and J. W. A. Robinson, Phys. Rev. Mater. **4**, 054414 (2020).
[52] L. Wang, Q. Feng, H. G. Lee, E. K. Ko, Q. Lu, and T. W. Noh, Nano Lett. **20**, 2468 (2020).
[53] A. Gerber, Phys. Rev. B **98**, 214440 (2018).
[54] R. Y. Chen, R. Q. Zhang, Y. J. Zhou, H. Bai, F. Pan, and C. Song, Appl. Phys. Lett. **116**, 242403 (2020).